We are IntechOpen, the world's leading publisher of Open Access books Built by scientists, for scientists

6,900
Open access books available

186,000
International authors and editors

200M
Downloads

Our authors are among the

154
Countries delivered to

TOP 1%
most cited scientists

12.2%
Contributors from top 500 universities

CLARIVATE ANALYTICS

BOOK CITATION INDEX

INDEXED

WEB OF SCIENCE™

Selection of our books indexed in the Book Citation Index
in Web of Science™ Core Collection (BKCI)

Interested in publishing with us?
Contact book.department@intechopen.com

Numbers displayed above are based on latest data collected.
For more information visit www.intechopen.com

6

Hydrogen in Ferroelectrics

Hai-You Huang, Yan-Jing Su and Li-Jie Qiao
University of Science and Technology Beijing
China

1. Introduction

It is well known that the ferroelectric random access memories (FRAM) as one of the most important applications of ferroelectric thin film have attracted much attention. However, the introduction of hydrogen into ferroelectric materials may cause severe degradations in dielectric properties, ferroelectric properties, optical properties and mechanical properties. Ferroelectricity is the most important property of ferroelectrics and the researches on hydrogen in ferroelectrics begin just from the effects on ferroelectric properties. Ferroelectric thin film is often integrated with existing Si technology to fabricate reliable nonvolatile memories. In Si technology, a forming gas (hydrogen containing gas) anneal at about 400 °C needs to carry on tying up dangling bonds at the Si/SiO_2 interface and reducing interface-trapped charges(Katz, 1988). Unfortunately, hydrogen could enter into ferroelectric thin film during annealing in forming gas and generates severe issue. For example, both $Pb(Zr,Ti)O_3$ (PZT) and $SrBi_2Ta_2O_9$ ferroelectric thin-film capacitors lose their polarization hysteresis characteristics as a result of such an anneal (Aggarwal et al., 1998; Shimanoto et al., 1997; Kushida-Abdelghafar et al., 1996; Han & Ma 1997).
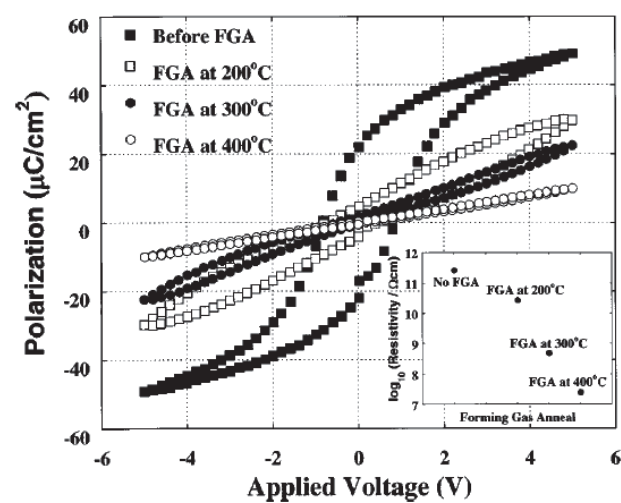
Besides the ferroelectricity, ferroelectric materials also have been wildly applied due to other important properties. Because that many ferroelectric ceramics, such as PZT and $BaTiO_3$, are excellent insulator against current, they are used to electric industry as capacitor. Hydrogen can increase leakage current and induce the insulator to a semiconductor (Huang et al., 2007 & Chen et al., 2011). Ferroelectric materials, especially its single crystals, have been widely used in optical devices because of its special optical properties such as photorefractive effect and nonlinear optical effect. Hydrogen can change the optical properties of ferroelectric materials (Wu et al., 2009). The mechanical property is another important property to sure ferroelectric devices could be used reliably. Hydrogen fissure (Peng et al., 2004) and hydrogen-induced delayed fracture (Huang et al., 2005; Zhang et al., 2008; Wang et al., 2003a, 2003b) could occur in some conditions.

This chapter reviews the effects of hydrogen on the properties of ferroelectric materials. This chapter is organized as follows: first of all, some background leading to the research interest of hydrogen in ferroelectric materials are introduced in section 1. In section 2 to 5, the effects of hydrogen on the ferroelectric properties (section 2), on the dielectric properties (section 3), on the optical properties (section 4) and on the mechanical properties (section 5) of ferroelectric materials are discussed in detail, respectively. In the end of this chapter, we conclude in section 6 where the important results of this research area are briefly summarized and outstanding problems and future directions are discussed.

2. Effects of hydrogen on ferroelectricity

2.1 Hydrogen reduces remanent polarization

In a ferroelectric material, there are lots of ferroelectric domains. The electric dipoles create by positive and negative bound charges in each domain are called spontaneous polarization vectors, which point to the positive poles of domains. Ferroelectric domain (polarization vector) can rotate 90° or 180° induced by applied force F or electric field E, known as domain switching. When the applied electric field is large enough all polarization vectors of domains have the same direction with the field, resulting in saturation polarization P_s. When the flied is removed, i.e., $E=0$, the polarization does not back to zero, but equals to remanent polarization P_r, that means a hysteresis effect of polarization. The hysteresis loop can be measured by change the field, as shown in Figure 1(Aggarwal et al., 1998 & Joo et al., 2002).

(a)
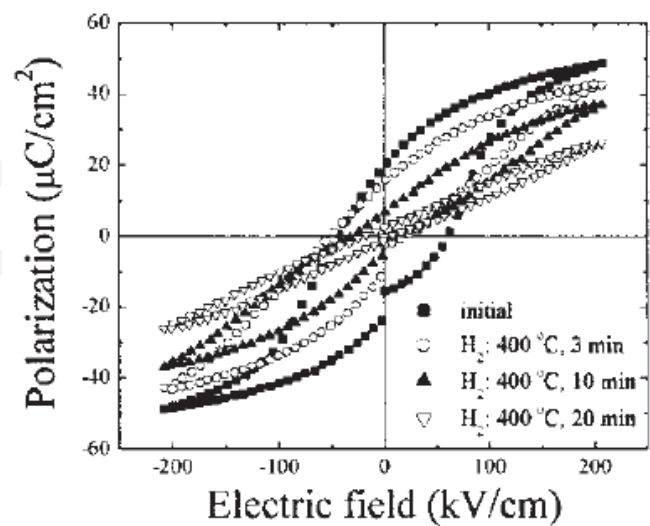
(b)

Fig. 1. Hydrogen charging causes hysteresis loop narrow and reduce the remanent polarization ((a)Aggarwal et al., 1998 & (b) Joo et al., 2002)

Ferroelectric materials have piezoelectricity, which is the generation of polarization charges as a result of applied stress or strain. The electric displacement vector D is proportional to the stress tensor T with a coefficient d, piezoelectric constant tensor. For perovskite structure ferroelectric materials, such as $BaTiO_3$ or PZT, piezoelectric constant tensor has only three independent components, $d_{15}=d_{24}$, $d_{31} = d_{32}$, d_{33}. Generally, d_{33} is used as the piezoelectric constant. Many experimental results have indicated that hydrogen caused a serious degradation of ferroelectric and dielectric properties of ferroelectric materials (Joo et al., 2002 ; Ikarashi, 1998 & Tamura et al., 1999). Charging of hydrogen could make the hysteresis loop narrow or disappear, i.e., make P_r decrease, as shown in Figure 1 (Aggarwal et al., 1998 & Joo et al., 2002). The hysteresis loops of PZT thin film capacitor with Pt electrode continuously narrowed after a annealing at 400 °C in a forming gas with 5% H_2 for 3 to 20 min, as shown in Figure 1b (Joo et al., 2002). With the annealing temperature increasing, the hysteresis loops also gradually narrowed and became a straight line at 400 °C (Aggarwal et al., 1998).
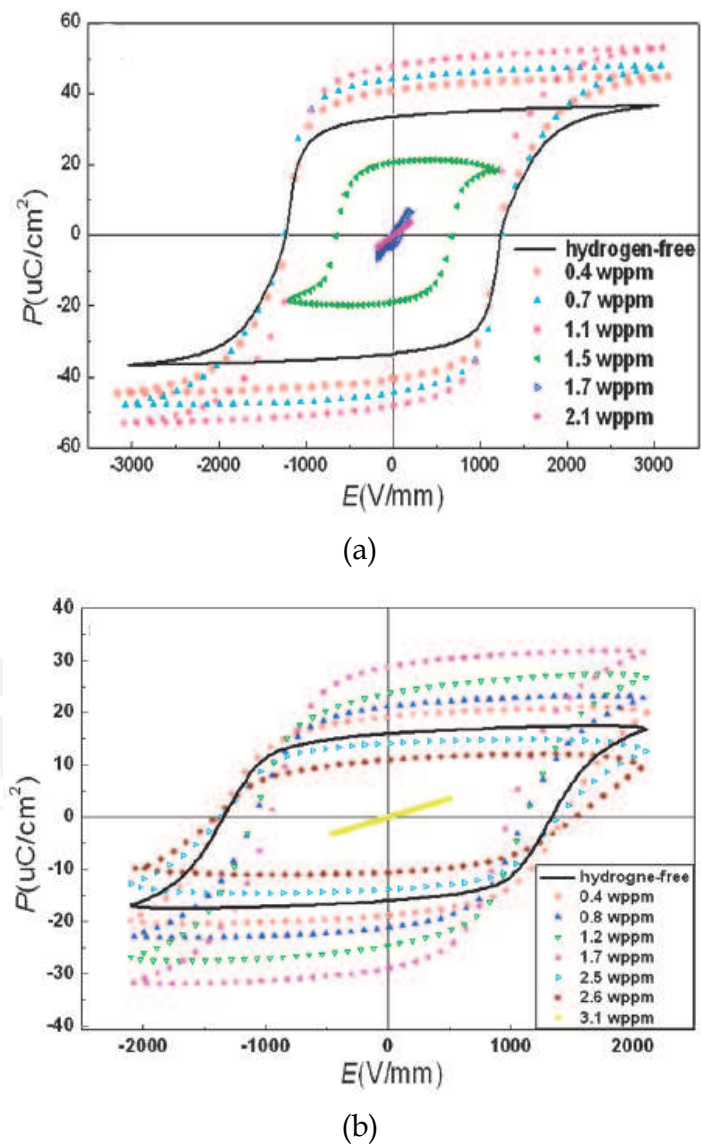

(a)

(b)

Fig. 2. The effects of hydrogen on hysteresis loops (a) PZT & (b) PZNT (Wu et al., 2010)

Our work shows that both for PZT and PZNT (91%PZN+9%PT), when hydrogen concentration in ferroelectric material, C_t, introduced by electrolysis or annealing in hydrogen gas is less than a critical concentration, C^* (for PZT, C^*=10 ppm and for PZNT, C^*=14 ppm), with the increase in hydrogen concentration, the hysteresis loop widens and P_r increases. However, when the hydrogen concentration is more than the critical value of C^*, hysteresis loop narrows and P_r falls with the increase in hydrogen concentration, as shown in Figure 2 (Wu et al., 2010). The effects of hydrogen concentration on P_r and d_{33} are shown in Figure 3 (Wu et al., 2010). When $C_t<C^*$, hydrogen can elevate both P_r and d_{33}. If $C_t>C^*$, P_r and d_{33} decrease sharply with the raise of C_t.
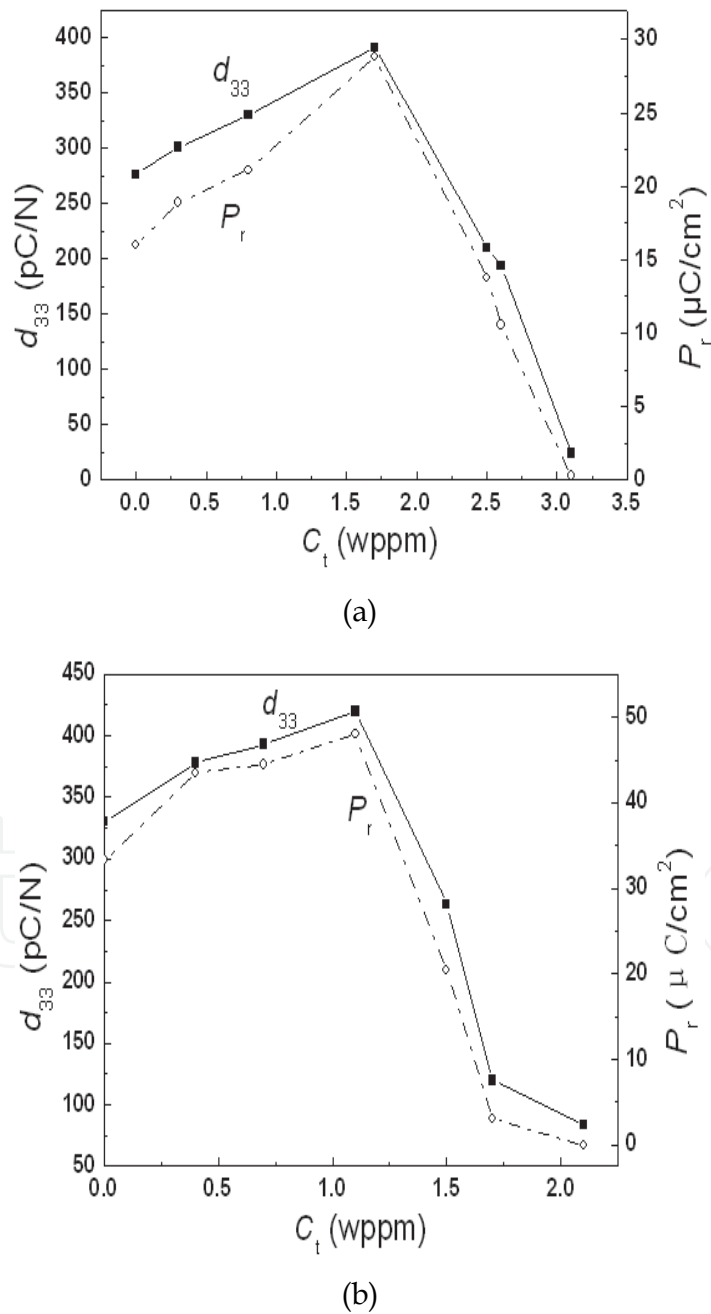

(a)

(b)

Fig. 3. The effects of hydrogen on P_r and d_{33} (a) PZT & (b) PZNT (Wu et al., 2010)

2.2 Hydrogen-hindered ferroelectric phase transition

The polarization-voltage hysteresis loop of PZT film disappeared gradually after forming gas annealing above its Curie temperature, as shown in Fig.1. No hysteresis implies that it is a cubic paraelectricity. Therefore, it seems that hydrogen entered above its Curie temperature can hinder the phase transition of the PZT film from cubic paraelectricity to tetragonal ferroelectricity.

X-ray diffraction (XRD) and heating differential scanning calorimetry (DSC) patterns of PZT ceramics in different charging conditions are shown in Figures 4a and 4b, respectively (Huang, et al., 2006). The appearance of double peaks in curves A, B, C, and E in Figure 4a corresponds to tetragonal phase and no double peaks in curve D corresponds to cubic phase. The ratios of c to a axis calculated based on curves A–E in Figure 4a were 1.0114, 1.0128, 1.0113, 1.0000, and 1.0077, respectively. The calculation of c/a also proves that curve D corresponds to cubic phase and the others correspond to tetragonal phase. Figure 4b indicates that there is an endothermic transition from tetragonal ferroelectricity to cubic paraelectricity at its Curie temperature of 300 °C for the samples uncharged and charged below the Curie temperature, as shown by curves A, B, and C in Figure 4b. For the sample charged in H_2 at 450 °C, however, there is no endothermic peak from 25 to 450 °C, as shown by curve D in Figure 4b. After outgassing at 800 °C, however, the endothermic peak appears again at the Curie temperature of 300 °C, as shown by curve E in Figure 4b. These results indicate that the lattice parameters and the tetragonal structure of the PZT do not change after charging at the temperature below the Curie temperature. However, if the charging temperature is higher than the Curie temperature, the PZT will be a cubic paraelectricity instead of tetragonal ferroelectricity after cooling to room temperature. After outgassing at 800 °C, the tetragonal ferroelectricity is restored. Therefore, hydrogen charged above its Curie temperature can hinder the phase transition from cubic to tetragonal during cooling to room temperature.

First principles plane-wave pseudopotential density functional theory was applied to calculate the effect of hydrogen on the ferroelectric phase transition in perovskite structure ferroelectricity based on energy calculation method. A hydrogen atom was put into the perovskite-type unit of cubic and tetragonal $PbTiO_3$ and then its possible locations were looked for. Figure 5a is a tetragonal $PbTiO_3$ with one H in the unit cell and A, B, and C are three possible sites H occupied. Calculation showed that the minimum values of total energies corresponding to site A at (0.5, 0.25, 0.05), tetrahedral interstitial site B at (0.25, 0.25, 0.25), and site C between Ti and apical O(1) ion at (0.5, 0.5, 0.25) were -4601.73, -4601.04, and -4600.15 eV, respectively. When hydrogen occupied site A, B, or C, the distances between H and O(1) were 0.1016 nm, 0.1485 nm, and 0.1529 nm, respectively. Hydrogen should occupy site A, the total energy is the lowest and the distance between H and O(1) has a smallest value, compared to sites B and C, which are the possible sites proposed by Aggarwal et al.(Aggarwal et al., 1998) The distance 0.1016 nm means that a strong interaction between H and O(1) exists, which can result in the overlap of the electronic clouds between H and O(1), as shown in Figure 5b. The calculation is consistent with the experimental results (Aggarwal et al., 1998 & Joo et al., 2002), i.e., existing O–H bonds in PZT ceramics. Calculation showed that the electron overlap populations between O–Ti were 0.98 for hydrogen-free $PbTiO_3$ and 0.70 for hydrogenated $PbTiO_3$, respectively. Hydrogen decreases the electron overlap population between O–Ti means that hydrogen weakens the interaction between O–Ti. It has been pointed out that the stronger the hybridization between the two atoms, the larger tendency to form bond or interaction between two atoms. Therefore, hydrogen decreases the overlap population between O–Ti and weakens the hybridization between O–Ti, resulting in the decrease of stability of tetragonal ferroelectric phase.
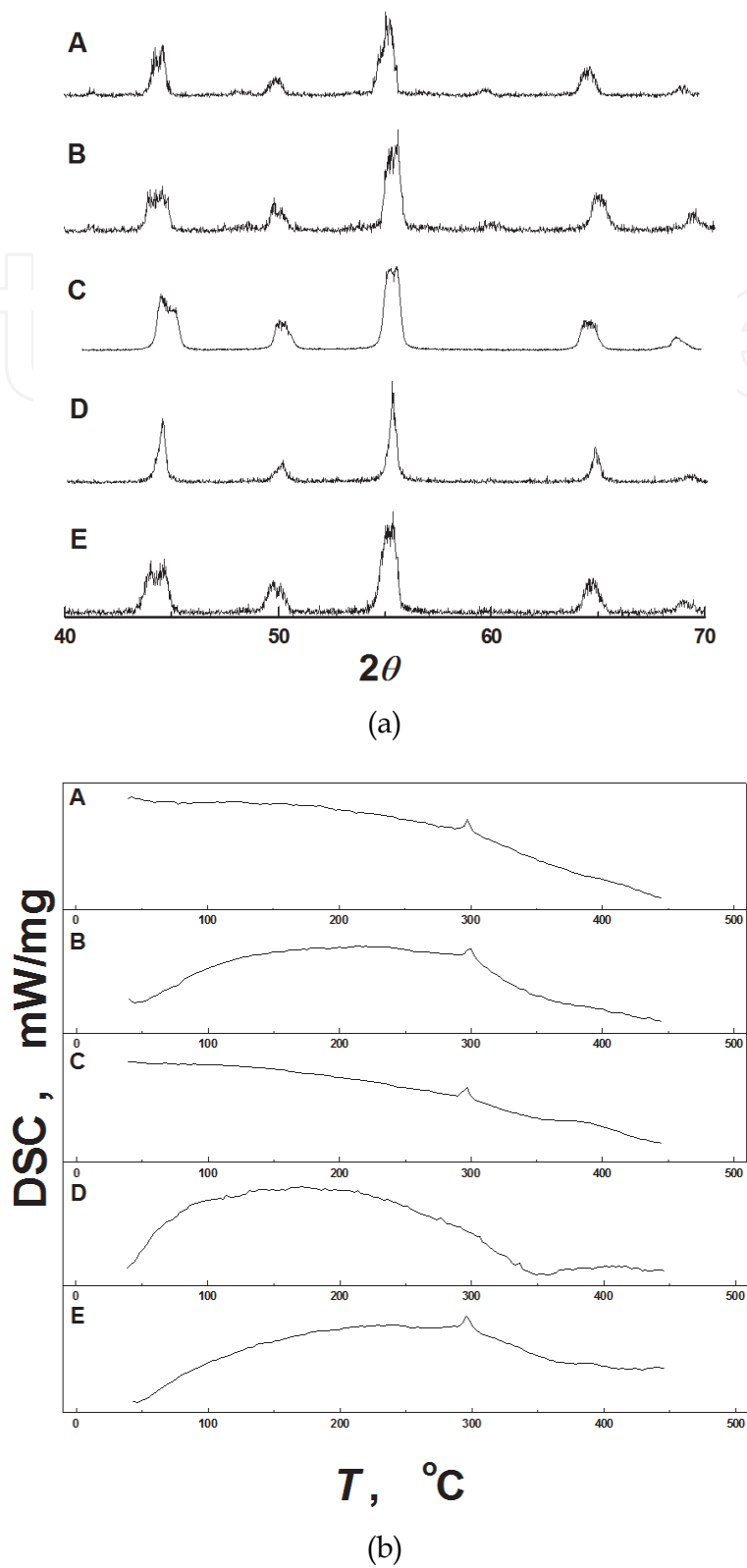
(a)

(b)

Fig. 4. XRD (a) and DSC (b) patterns of PZT-5H in different charging conditions A, hydrogen-free; B, charging at 400 mA/cm² in solution at 20℃ ; C, charging in H₂ at 250℃; D, charging in H₂ with P_{H_2} =0.4 MPb at 450 ℃; E, outgassing at 800℃ after charging in H₂ at 450℃ (Huang, et al., 2006)
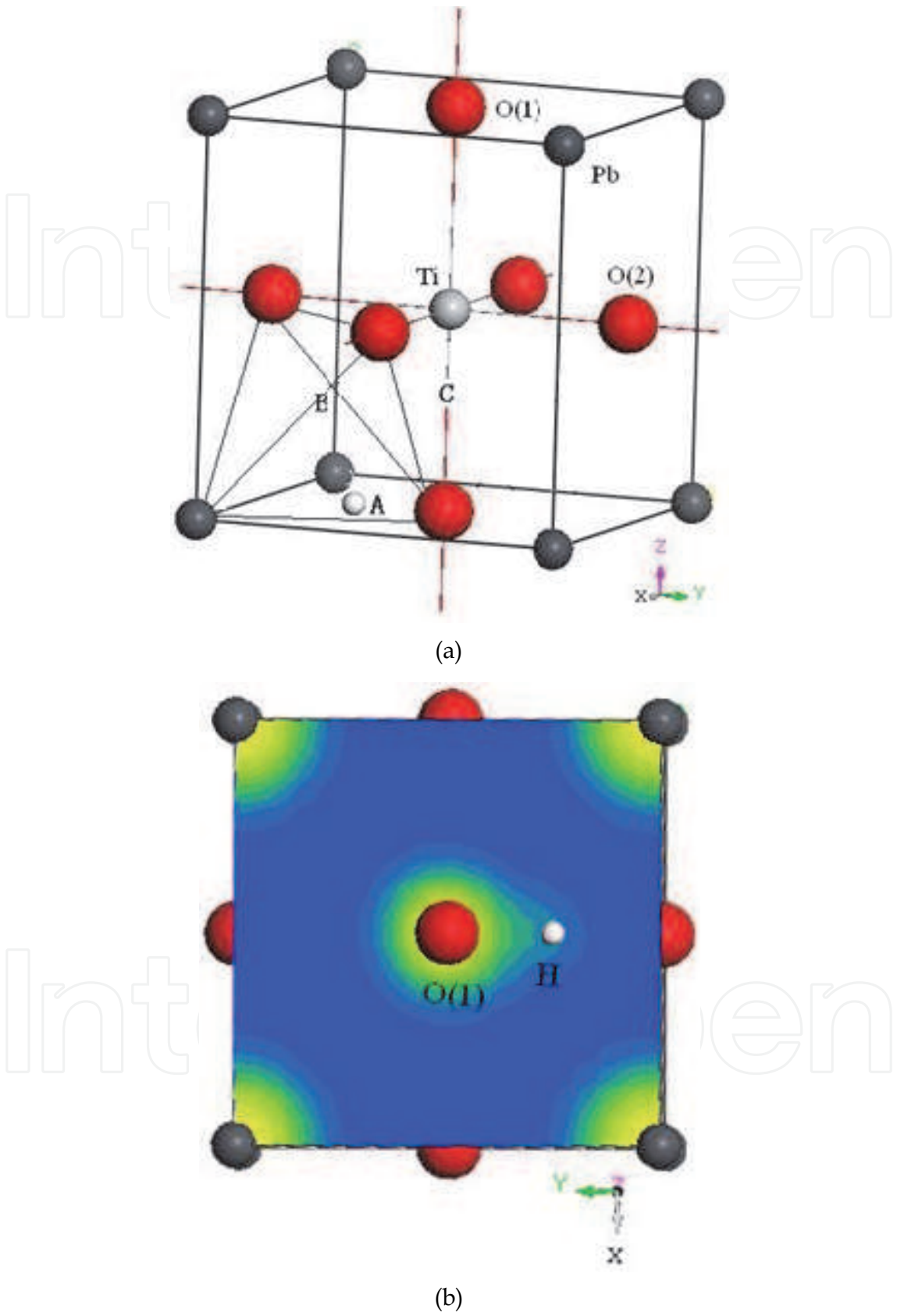
(a)

(b)

Fig. 5. Unit cell of tetragonal $PbTiO_3$ containing one hydrogen atom (a), and electronic clouds of XOY plane (b) (Huang, et al., 2006)

The variation of the total energy with the displacement of Ti along the c axis for hydrogen-free and hydrogenated $PbTiO_3$ is shown in Figure 6. Figure 6a indicates that for hydrogen-free $PbTiO_3$ with the tetragonal structure, there are two lowest energy sites for Ti in the c axis which are ±0.016 nm from the center of the unit cell. The calculation result is consistent with the experimental value of ±0.017 nm. Figure 6b, however, shows that for the hydrogenated tetragonal structure, the double-lowest-energy sites of Ti along the c axis disappear and the lowest energy site located at the center of the cell. Therefore, when hydrogen enters into the cubic $PbTiO_3$ above its Curie temperature, the cubic structure continues to be a stable structure during cooling because for Ti there is no lower energy site than the center of the cell. As a result, ferroelectric tetragonal structure in $PbTiO_3$ charged above the Curie temperature will not appear during cooling to room temperature because of no displacement of Ti along the c axis. The calculation can explain the experiment that hydrogen charged above its Curie temperature will hinder phase transition of PZT from cubic paraelectricity to tetragonal ferroelectricity.

Figure 4, however, also indicates that PZT keeps a tetragonal structure after charging at the temperature below the Curie temperature. The reason is the existence of energy barrier from tetragonal to cubic which composed of elastic energy, depoling energy, and static electric energy. Besides the insufficient thermal energy, hydrogen entered into tetragonal PZT during charging below the Curie temperature cannot provide an additive energy to overcome the energy barrier, and then the tetragonal structure cannot transform to cubic structure during charging below the Curie temperature.
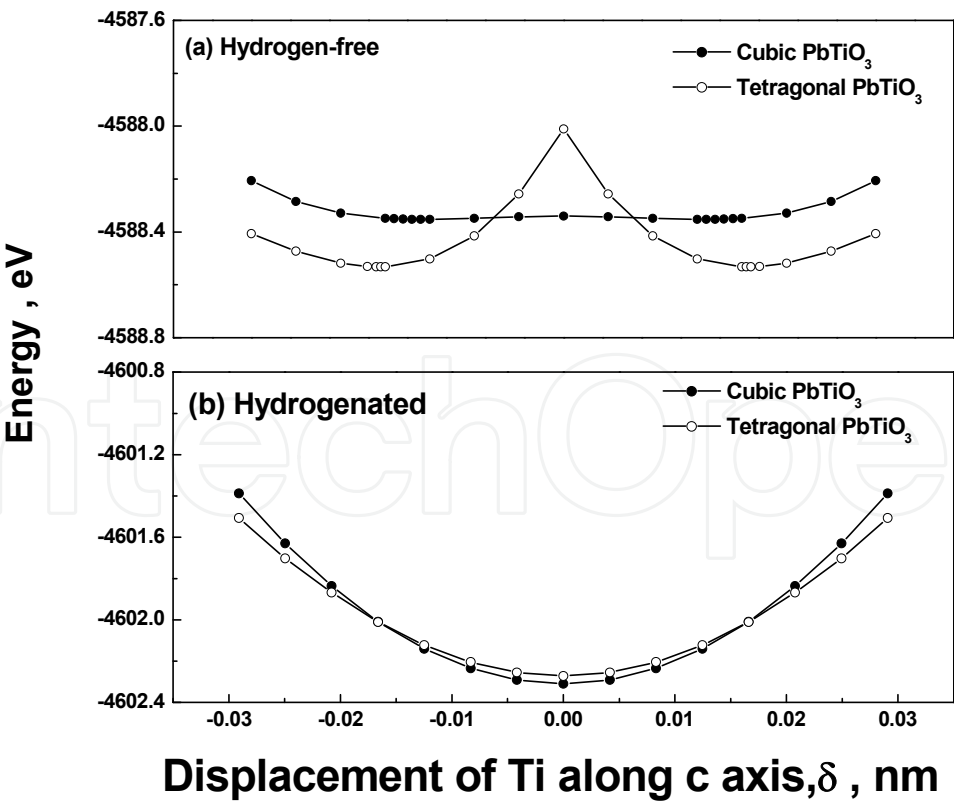

Fig. 6. Total energy vs. displacement of Ti along c axis, the original is the centre of the cell (a) hydrogen-free $PbTiO_3$, (b) hydrogenated $PbTiO_3$ (Huang, et al., 2006)

3. Hydrogen induced semiconductor transformation of ferroelectrics

Ferroelectric or piezoelectric ceramics, such as PZT, is an insulator. However, after annealing in a forming gas containing H_2 or electrode plating process, hydrogen can enter into the ceramics and makes its resistivity from 10^{12}-10^{13} Ω·cm down to 10^6-$10^7\Omega$·cm sharply, resulting in becoming a semiconductor (Han & Ma, 1997). The resistivity and capacitance of multilayer ferroelectric ceramic capacitors degrade to a semiconductor and the dielectric loss increases after hydrogen charging in NaOH (Chen et al., 1998). Figure 7a illustrates the leakage current in PZT ceramics increased sharply after electrolysis or hydrogen gas charging. The semiconductorization of ferroelectric ceramics by hydrogen can be restored by outgassing. For example, after outgassing of hydrogen at a temperature higher than 400 °C, the hydrogenated PZT restores an insulator, as shown in Figure 7b (Huang et al., 2007). A very few hydrogen can lower the resistivity of PZT from 10^{13} Ω·cm to 10^8 Ω·cm. carrier concentration increases rapidly with the raise of hydrogen concentration (Huang et al., 2007). Hall effect measurements show that PZT ceramics change into n-type semiconductor after hydrogen charging (Huang et al., 2007).
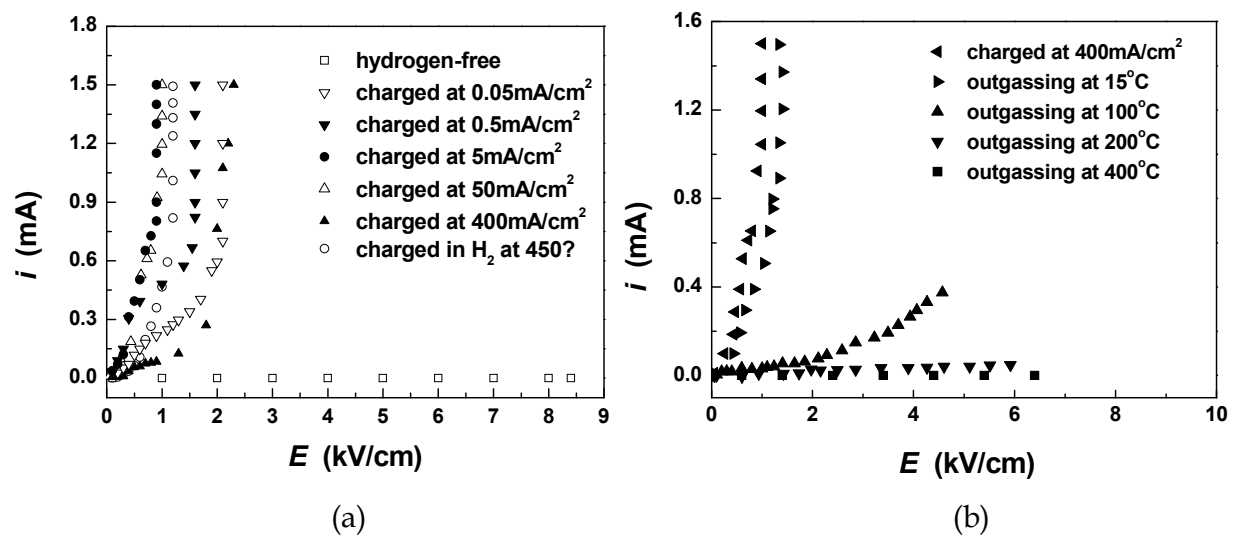

Fig. 7. The effects of hydrogen charging (a) and outgassing (b) on the leakage current in PZT (Huang et al., 2007)

The first principles calculation was applied to investigate the effect of hydrogen on the conductivity of ferroelectric materials. The variations of density of states of every atom in PZT with energy difference E-E_F (E_F is Fermi energy) were calculated (Wu, 2009). If not hydrogen, the total density of states of all atoms in PZT vs E-E_F, as shown in Figure 8a, where AB is the valence band, BC is the forbidden band and CD is the empty band. If the hydrogen concentration C_H=1536 wppm, the whole curve move to low energy (left) after hydrogen charging, so that the energy of parts of the empty band is less than the Fermi energy and becomes the bottom of conduction band, which was filled by electrons mainly from H 1S (Ti, Pb, Zr also contribute them free electrons). As a result, the forbidden band does no longer exist and the material becomes a conductor, as shown in Figure 8b. When C_H reduces to 770 wppm, the energy of parts of the empty band is still below the Fermi energy and it is still a conductor, as shown in Figure 8c. When C_H=96 wppm, all empty band higher than the E_F, so there is a narrow band gap that means the material becomes a

semiconductor, as shown in Figure 8d. For PZT, no matter what method of hydrogen charging was applied, saturation hydrogen concentration is less than 96 wppm. Thus, it is impossible to make PZT to a conductor by hydrogen charging, but hydrogen can make PZT into a semiconductor.
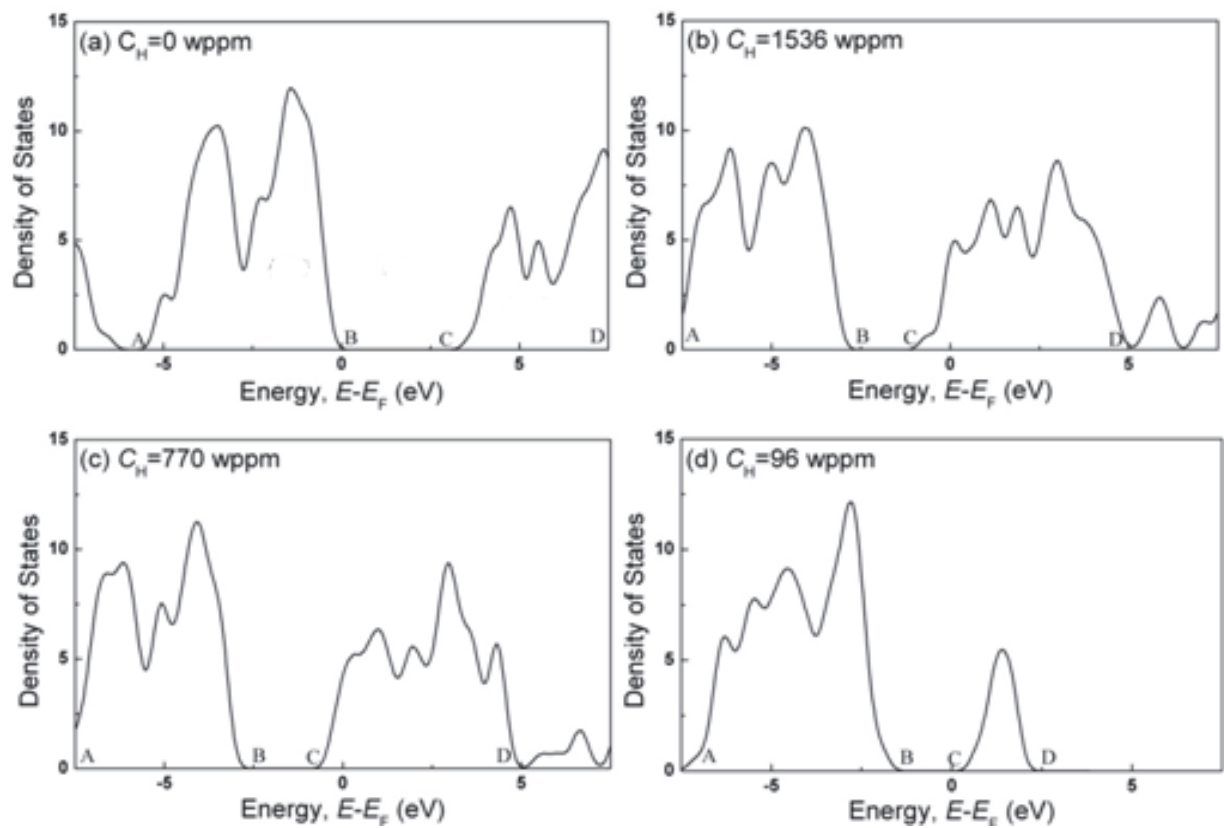

Fig. 8. Density of states for PZT with different C_H (Wu, 2009)

Why hydrogen charging make the PZT into a semiconductor from an insulator. One view is that H can react with O^{2-} to form H_2O and oxygen vacancy with two electrons V(2e) (Chen et al., 1998), i.e.,

$$2H+O^{2-}=H_2O+V(2e) \tag{1}$$

The two electrons of oxygen vacancy can ionize and induce insulating ferroelectric ceramic to be semiconductor. However, because H_2O molecule is too large to locate in the lattice, the reaction (1) can only occur on the surface of ferroelectric ceramic and make the reaction to continue through migration of O^{2-} to the surface. Nevertheless, the diffusion coefficient of O is very small in the ceramics at room temperature (in $BaTiO_3$ at room temperature $D_O=1.1\times10^{-15}$ cm²/s) (Huang et al., 2007). Considering hydrogen charging for 45h at room temperature, the maximum diffusion distance is only 0.53 µm. However, the experimental value of transition distance is up to 0.9 mm (see Figure 9), which is 10^3 times as large as the calculative maximum diffusion distance of O (Huang et al., 2007) . Another view is that a part of PbO reduced to Pb by H, i.e., (Han & Ma, 1997)

$$2H+PbO=H_2O+Pb \tag{2}$$

A small amount of Pb can become the ceramics into the semiconductor. For the same reason, the reaction can't be achieved kinetically. Figure 8 shows that 1S electron of H can across the band gap and into conduction band, such as if C_H>96 ppm, the electrons in the bottom of conduction band (mainly from H 1S) to become a conductor. In fact, the C_H<96 ppm, so the hydrogen charging is impossible to make PZT be a conductor. However, the density of states of hydrogenated ferroelectric ceramics moves to left and narrows the band gap to a lever of semiconductor. 1S electron of H can be as free electron and degrade the electrical resistivity drastically.

4. Effects of hydrogen on optical properties

After hydrogen charging, the color of PZT became black (Chen et al., 1998 & Joo et al. 2002). Beside PZT, for $BaTiO_3$ single crystals, the color became darker and is absent transparent after hydrogen charging, as shown in Figure 9 (Huang et al. 2007 & Wu et al. 2009). The darker color means more visible light are absorbed. The experiments show that the absorption coefficient of PZT and $BaTiO_3$ within visible region significantly heighten after hydrogen charging, as shown in Figure 10 (Wu et al. 2009).

The phenomena of hydrogen changing the color of PZT can be used to measure the diffusion coefficient of hydrogen in PZT. 0.9 mm-thick PZT sample was charged of hydrogen from single side for 2.5h, 10h, 20h and 45h. The cross section of hydrogenated sample was shown in Figure 11a, and the average diffusion distance of hydrogen x for different charging time t can be measured, as shown in Figure 11b. Based on the linear relationship between x and $t^{1/2}$, i.e., $x=4\sqrt{Dt}$, the diffusion coefficient of hydrogen in PZT D=4.9×10^{-8} cm^2/s at room temperature can be obtained (Huang et al. 2007).
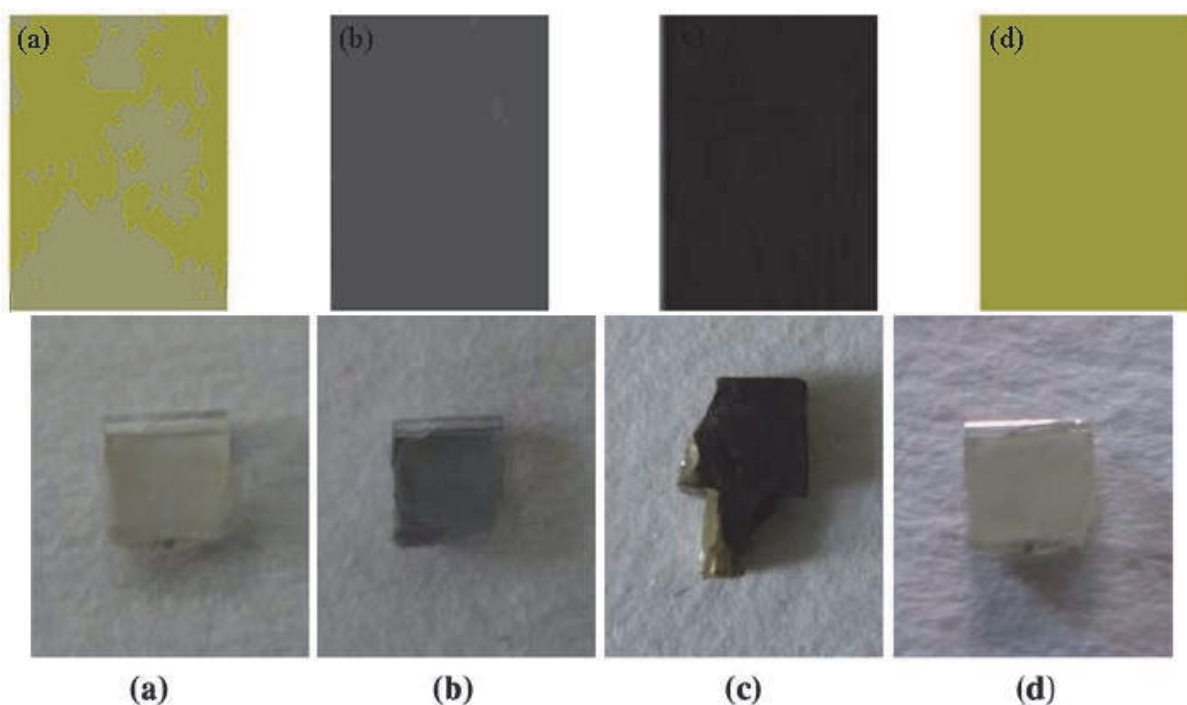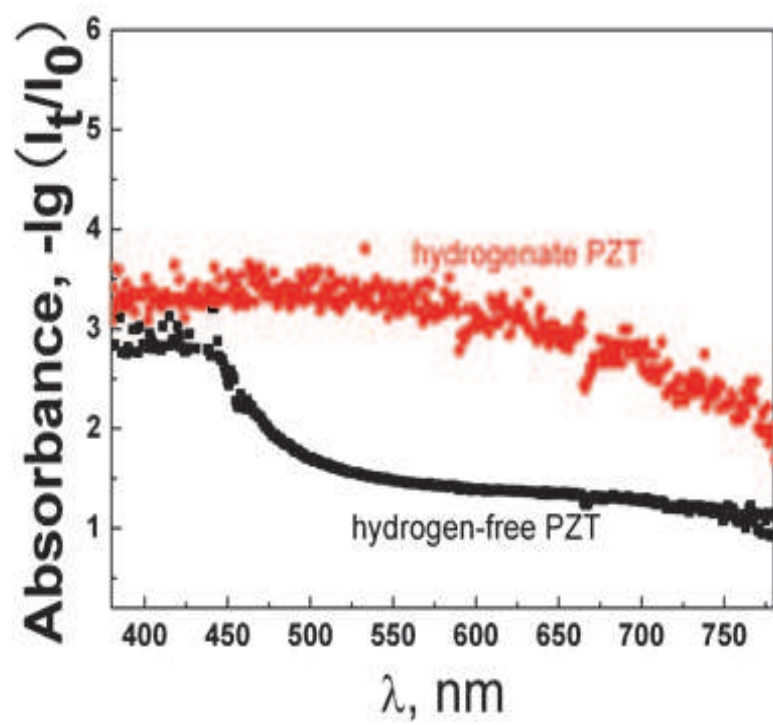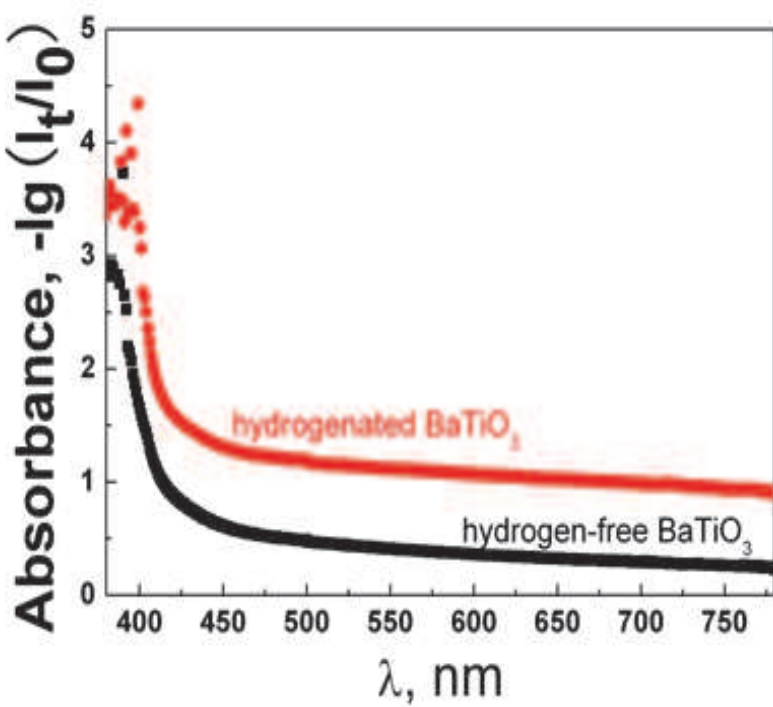

Fig. 9. The color changes of PZT (upper) and $BaTiO_3$ (lower) before and after hydrogen charging (a) before hydrogen charging, (b) electrolytically charged, (c) charged in H_2 gas, (d) outgassing after charging (Huang et al. 2007 & Wu et al. 2009)

(a)

(b)

Fig. 10. Hydrogen increases the absorption coefficient within visible region (a)PZT & (b)BaTiO$_3$ (Wu et al. 2009)
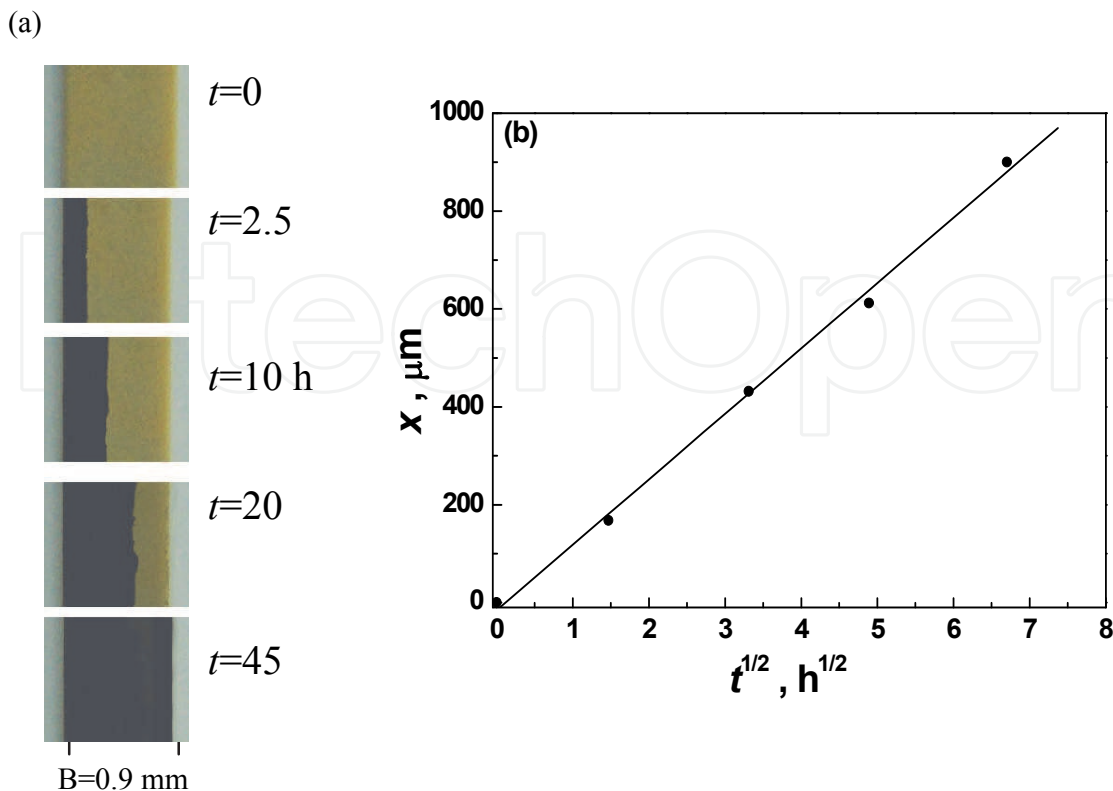
(a)

Fig. 11. Diffusion of hydrogen in PZT ceramics (a) color change and (b) diffusion distance at different time (Huang et al. 2007)

5. Hydrogen induced cracking

5.1 Hydrogen fissure in PZT ferroelectric ceramics without loading

Three groups of PZT ferroelectric ceramics were used to investigate hydrogen fissure without any loading. The group I samples were polarized by a high electric field (30kV/cm) at room temperature and a large internal stress was induced. The group II samples were polarized at high temperature (400 ˚C, higher than the Curie point) by a small electric field (2kV/cm), and then furnace cooled to room temperature, in which there was little internal stress. The third group of samples was not polarized. We called the three groups of samples as HP, SP and UP samples, respectively. Hydrogen charging was carried out for all samples in a 0.2mol/l NaOH +0.25 g/l As$_2$O$_3$ solution with various current densities i. For the HP samples, appeared four discontinuous microcracks like a, b, c and d appeared on the surface after hydrogen charging with i=5 mA/cm^2 for 4h, as shown in Figure 12 (Peng et al., 2004). These microcracks initiated and grew along the grain boundaries. Experiment showed that no hydrogen fissure was found after charging for 48h when i=0.05 mA/cm^2, but when i≥0.5mA/cm^2, after a certain incubation period, hydrogen fissure can form. However, for SP samples and UP samples, when i≤300 mA/cm^2, on hydrogen fissure formed for 48 h. hydrogen fissure appeared until i=400 mA/cm^2, as shown in Table 1 (Peng et al., 2004). In order to measure hydrogen concentration C_H, some samples were charged for 100 h with various current densities, and then put into a glass tube filled with silicon oil. The C_H can be calculated by Eq.3 based on the saturation volume of hydrogen V(cm3).

$$C_H(wppm)=10^6 \times 2n(g)/m(g)=2 \times 10^{-6} V(cm^3)/82.06m(g)T(k) \qquad (3)$$

where $n(g)=PV/RT=V(cm3)/82.06T(K)$ is the molar number of hydrogen under 1 atm, $m(g)$ is the weight of the sample and $T(K)$ is temperature. The values of C_H corresponding to various i were also listed in Table 1
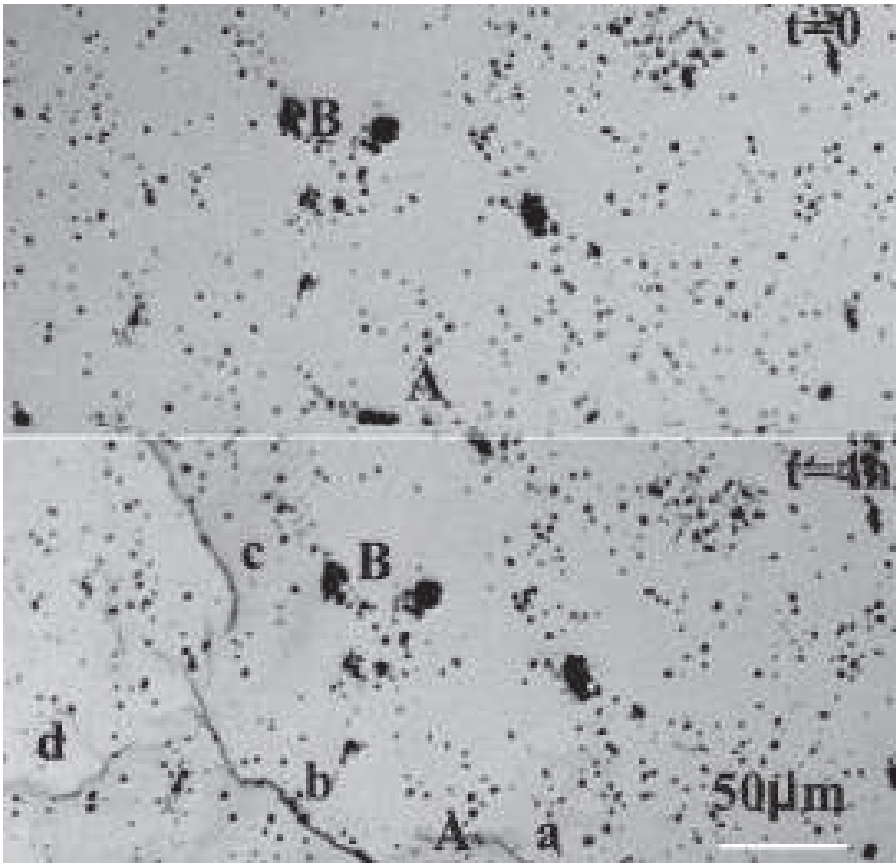

Fig. 12. Hydrogen fissure after charging at 5 mA/cm² for 4 h; a to d are fissures, and A and B are marks for location (Peng et al., 2004)

i, mA/cm²	0.05	0.5	5	50	300	400
C_H, wppm	0.92	2.61	4.8	7.16	9.84	10.3
HP samples	no	yes	yes	yes	yes	--
SP samples	no	no	no	no	no	yes
UP samples	no	no	no	no	no	yes

Table 1. Hydrogen concentration and fissure appearance corresponding to various charging current densities (Peng et al., 2004)

There are many cavities and microholes in the grain boundary of sintered PZT ceramics. During hydrogen charging H atoms enter into the holes and generate H_2, which can induce an internal pressure P. When the hydrogen pressure is large enough, the normal stress on the holes wall $P/2$ equals to the cohesive strength $\sigma_{th}(H)$ at grain boundary,

which has been reduced by atomic hydrogen, hydrogen fissure or microcrack will form. If there is a extra internal stress σ_i, the critical hydrogen pressure for cracking can be decreased from $P=2\sigma_{th}(H)$ to $P^*=2\sigma_{th}(H)-\sigma_i$. Because there is a large internal stress in HP sample, which can promote crack nucleation, so hydrogen fissure appear when $i=0.5mA/cm^2$. The microcracks are found in SP and UP samples only when $i=400$ mA/cm² for absence of internal stress.

5.2 Hydrogen reduce fracture toughness of ferroelectric material

Vickers indentation was carried out on the surfaces of three ferroelectric ceramic samples to obtain indentation fracture toughness K_{IC} according to Eq.4.

$$K_I = 0.0638P / d\sqrt{l} \qquad (4)$$

where P is the load, d is diagonal length of the indentation and l is the crack length. Then, the samples with indentation cracks were charged into 4.1 ppm, 8.1 ppm and 12.1 ppm hydrogen, respectively. Unloaded indentation cracks can grow induced by the indentation residual stress during charging. The indentation crack length after hydrogen charging was measured to calculate the threshold stress intensity factor of hydrogen-induced delayed cracking (HIDC), K_{IH}, by Eq.4. New indentations were carried out on the surface of hydrogenated samples. The fracture toughness for hydrogenated sample $K_{IC}(H)$ can also be obtained. The experiments indicated that both K_{IH}/K_{IC} and $K_{IC}(H)/K_{IC}$ decreased linearly with the increasing C_H, as shown in Figure 13 (Zhang et al., 2008).
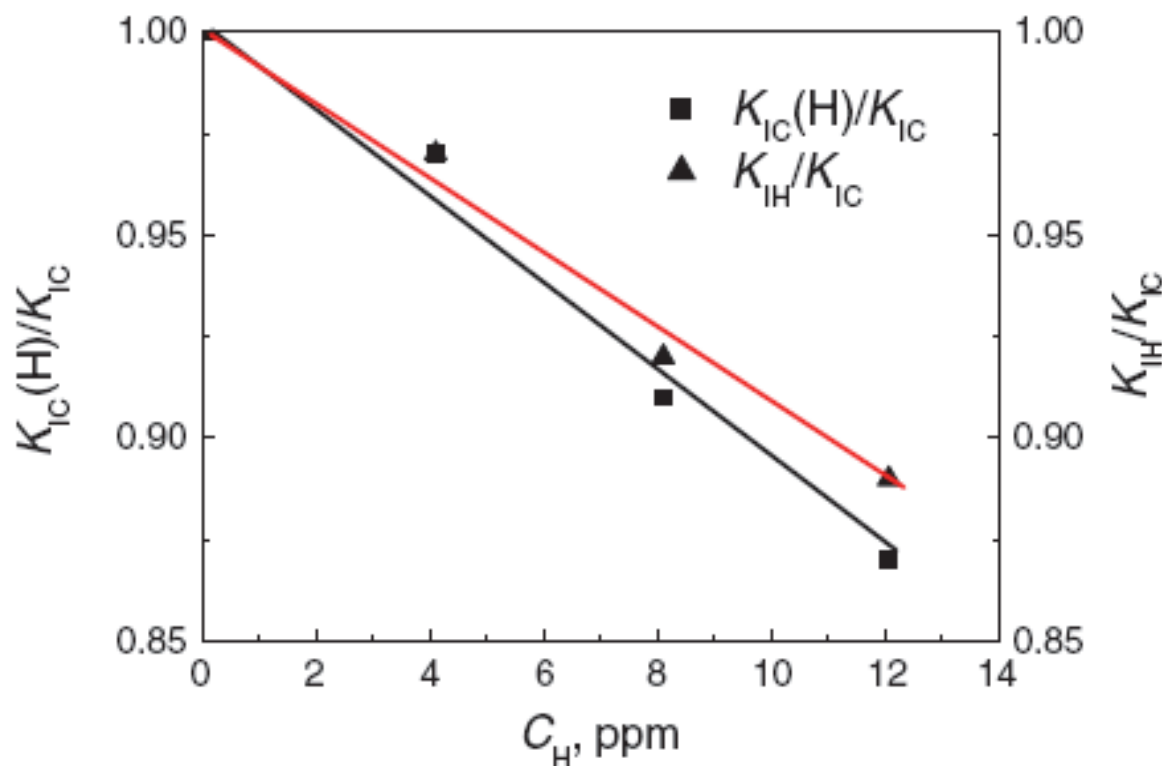

Fig. 13. Hydrogen concentration dependence of the relative fracture toughness of charged samples, K_{IH}/K_{IC}, and of the normalized threshold stress intensity factor of hydrogen-induced cracking induced by residual stress, $K_{IC}(H)/K_{IC}$ (Zhang et al., 2008)

The crack length increased with increasing hydrogen concentration in the samples. Therefore, the cracks can also grow with the prolongation of dwell time during indentation test in a pre-charged sample since the hydrogen concentration will increase at the indentation crack tips by stress-induced diffusion. The experimental results indicate that the longer the indentation load hold, the larger the indentation crack length is, and the smaller fracture toughness, $K_{IC}(H,t)$ measures, as shown in Figure 14 (Zhang et al., 2008). Under a constant load, the HIDC can occur by the stress-induced hydrogen diffusion and enrichment.
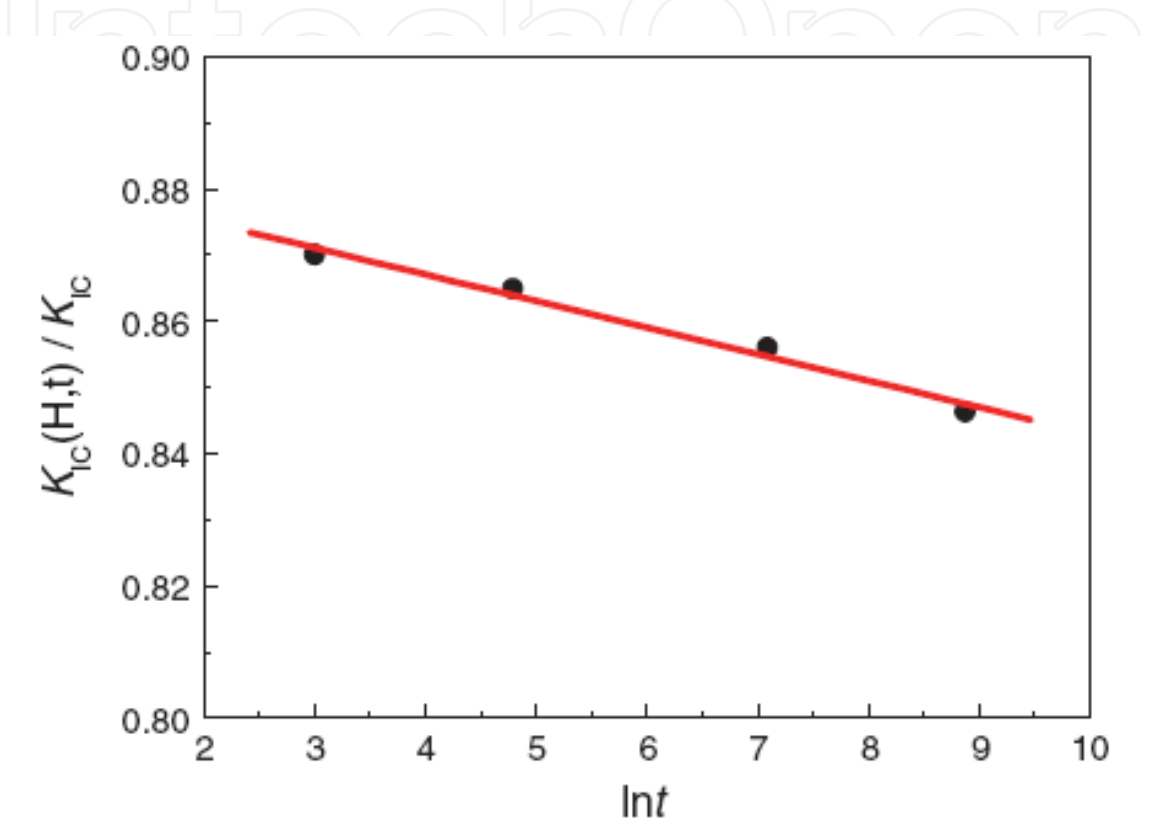
Fig. 14. The normalized fracture toughness $K_{IC}(H,t)/K_{IC}$ versus the logarithm of the dwell time during the indentation test for the charged sample (Zhang et al., 2008)

5.3 Hydrogen-induced delayed cracking in ferroelectric ceramics
During single-edge-notched-tensile sample of PZT ferroelectric ceramics hydrogen charging dynamically in 0.2mol/l NaOH+0.25 g/l As$_2$O$_3$ solution, hydrogen-induced delayed cracking (HIDC) can occur (Wang et al., 2003a) and depends on the relative orientation between notch plane and the polarization vector, i.e., the HIDC also shows anisotropy in ferroelectric ceramics, as shown in Figure 15 (Wang et al., 2003b). Hydrogen concentration C_H under different charging current densities is given in Table 2. The curve of K_{IH}/K_{IC} vs i or C_H can plot based on Table 2 and one can find a linear relationship between K_{IH}/K_{IC} and the lnC_H (Wang et al., 2003b)

$$K_{IH}^a / K_{IC}^a = K_{IH}^b / K_{IC}^b = 0.4\text{-}0.15\ln C_H \tag{5}$$

where superscript a and b denote polarization vector parallel and perpendicular to the crack plane, respectively. K_{IC}^a =1.53 MPam$^{1/2}$ and K_{IC}^b =1.12 MPam$^{1/2}$ for PZT ferroelectric

i (mA/cm²)	0.05	0.5	5	50	300
C_H(ppm)	0.92	2.61	4.8	7.16	9.84
K_{IH}^a (MPam$^{1/2}$)	0.54	0.34	0.28	0.13	0.01
K_{IH}^b (MPam$^{1/2}$)	0.36	0.26	0.17	0.08	-
K_{IH}^a / K_{IC}^a	0.40	0.25	0.21	0.10	0.01
K_{IH}^b / K_{IC}^b	0.40	0.28	0.19	0.09	-

Table 2. The threshold stress intensity factors of HIDC corresponding to various hydrogen concentrations (Wang et al., 2003b)
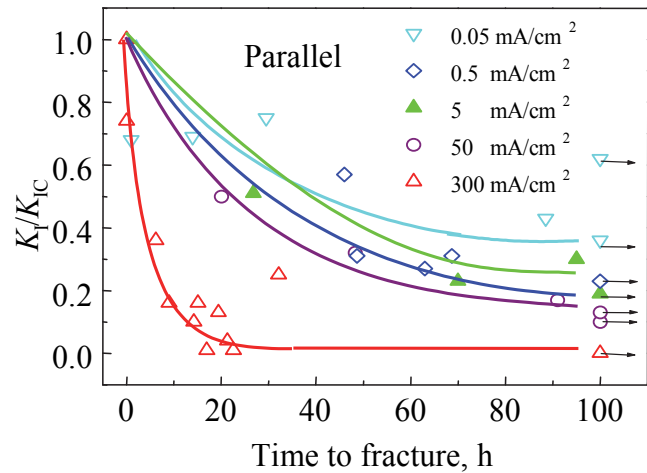
(a)
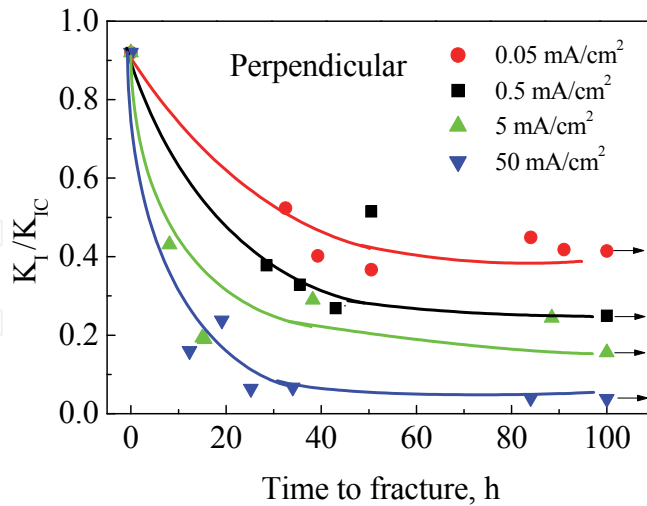
(b)

Fig. 15. The normalized stress intensity factor vs time to fracture during dynamically charging with various i (the arrows mean no fracture within 100 h). (a) Polarization direction parallel to the crack plane; (b) Polarization direction perpendicular to the crack plane (Wang et al., 2003b)

ceramics. Eq.5 suggests that the *t* anisotropy of K_{IH} is entirely caused by the anisotropy of fracture toughness.

6. Conclusion

In this chapter, the effects of hydrogen on main properties of ferroelectric materials are reviewed. Even if a little amount of hydrogen enters a ferroelectric material, the ferroelectricity and dielectric properties would be degraded, such as hydrogen causes hysteresis loop narrower, reduces remnant polarization, increases leakage current, etc. If great amount hydrogen is charged into ferroelectrics, hydrogen fissure and hydrogen-induced delayed cracking can occur. Fortunately, hydrogen can escape from the hydrogenated ferroelectric materials and properties can restore after a heat treatment. Therefore, outgassing treatment is an effectual method to prevent hydrogen damage. Although most of reports about hydrogen in ferroelectrics proved that hydrogen has negative influence, hydrogen can't be consider completely harmful to the ferroelectric materials. For example, a very small amount of hydrogen can enhance the ferroelectricity. Now, the mechanism of enhancement effect is not clear yet, but this phenomenon enough to absorb more interests to develop the potential role of hydrogen in ferroelectric materials.

7. Acknowledgment

8. References

Aggarwal, S.; Perusse, S. R.; Tipton, C. W.; Ramesh, R.; Drew, H. D.; Venkatesan, T.; Romero, D. B.; Podobedov, V. B. & Weber, A. (1998). Effect of hydrogen on Pb(Zr,Ti)O$_3$-based ferroelectric capacitors. *Applied Physics Letters*, Vol.73, No.14, pp. 1973-1975, ISSN 0003-6951

Chen, F.; Chen, W. P.; Wang, Y.; Hu, Y. M.; Shen, Z. J. & Chan, H. L. W. (2011). Effects of forming gas annealing on LiNbO3 single crystals. *Physica B: Condensed Matter*, Vol. 406, No.3, pp. 683-686, ISSN 0921-4526

Chen, W. P.; Li, L. T.; Qi, J Q. & Gui Z. L. (1998). Effect of electrochemical hydrogen charging on Ba1-xPbxTiO3-Based semiconducting ceramics. *Journal of Materials Science Letters*, Vol.17, No.11, pp.899-900, ISSN 0261-8028

Joo, H. J.; Lee, S. H.; Kim, J. P.; Ryu, M. K. & Jang, M. S. (2002). Effect of hydrogen on the electrical and optical properties in ferroelectric Pb(Zr,Ti)O$_3$ thin films. *Ferroelectrics*, Vol.272, No.1, pp.149-154, ISSN 1563-5112

Han, J. P. & Ma, T. P. (1997). Electrode dependence of hydrogen-induced degradation in ferroelectric Pb(Zr,Ti)O$_3$ and SrBi$_2$Ta$_2$O$_9$ thin films. *Applied Physics Letters*, Vol.71, No.9, pp. 1267-1269, ISSN 0003-6951

Huang, H. Y.; Chu, W. Y.; Su, Y. J.; Qiao, L. J. & Gao, K. W. (2005). Combined effect of electric field and residual stress on propagation of indentation cracks in a PZT-5H

ferroelectric ceramic. *Materials Science and Engineering B*, Vol. 122, No.1, pp. 1-6, ISSN 0921-5107

Huang, H. Y.; Chu, W. Y.; Su, Y. J.; Li, J. X.; Qiao, L. J. & Shi, S. Q. (2006). Experiment and first principles investigation on the hydrogen-hindered phase transition of ferroelectric ceramics. *Applied Physics Letters*, Vol.89, No.142904, ISSN 0003-6951

Huang, H. Y.; Chu, W. Y.; Su, Y. J.; Gao, K. W.; Li, J. X. & Qiao, L. J. (2007). Hydrogen-induced semiconductor transformation of PZT ferroelectric ceramics. *Journal of the American Ceramics Society*, Vol. 90, No.7, pp. 2062 – 2066, ISSN 0002-7820

Ikarashi, N. (1998) Analytical transmission electron microscopy of hydrogen-induced degradation in ferroelectric Pb(Zr,Ti)O$_3$ on a Pt Electrode. *Applied Physics Letters*, Vol.73, No.14, pp.1955-1957, ISSN 0003-6951

Katz, L. E. (1988). In: VLSI Technology (2nd ed), S. M. Sze (Ed), pp. 127, McGraw-Hill, ISBN 978-007-0627-35-2, New York

Kushida-Abdelghafar, K.; Miki, H.; Torii, K. & Fujisaki, Y. (1996). Electrode-induced degradation of Pb(Zr$_x$Ti$_{1-x}$)O$_3$ (PZT) polarization hysteresis characteristics in Pt/PZT/Pt ferroelectric thin-film capacitors. *Applied Physics Letters*, Vol.69, No.21, pp. 3188-3190, ISSN 0003-6951

Pen, X.; Su, Y. J.; Gao, K. W.; Qiao, L. J. & Chu, W. Y. (2004). Hydrogen fissure in PZT ferroelectric ceramic, *Materials Letters*, Vol.58, No.15, pp. 2073-2075, ISSN 0167-577x

Shimamoto, Y.; Kushida-Abdelghafar, K.; Miki, H. & Fujisaki, Y. (1997). H$_2$ damage of ferroelectric Pb(Zr,Ti)O$_3$ thin-film capacitors-The role of catalytic and adsorptive activity of the top electrode. *Applied Physics Letters*, Vol.70, No.23, pp. 3096-3097, ISSN 0003-6951

Tamura, T.; Matsuura, K.; Ashida, H.; Kondo, K. & Otani, S. (1999). Hysteresis variations of (Pb,La)(Zr,Ti)O3 capacitors baked in a hydrogen atmosphere. *Applied Physics Letters*, Vol.74, No. 22, pp.3395-3397, ISSN 0003-6951

Wang, Y.; Chu, W. Y.; Qiao, L. J. & Su, Y. J. (2003a). Hydrogen-induced delayed fracture of PZT ceramics during dynamic charging under constant load，*Materials Science and Engineering B*, Vol. 98, No.1, pp. 1-5, ISSN 0921-5107

Wang, Y.; Chu, W. Y.; Su, Y. J.; Qiao, L. J. & Gao, K. W. (2003b)，Hydrogen-induced cracking and its anisotropy of a PZT ferroelectric ceramics，*Science in China E*, Vol.46, No.3, pp.318-325, ISSN 1674-7321

Wu, M.; Huang, H. Y.; Jiang, B.; Chu, W. Y.; Su, Y. J.; Li, J. X & Qiao, L. J. (2009). Experiments and first principles calculations on the effects of hydrogen on the optical properties of ferroelectric materials. *Journal of Materials Science*, Vol. 44, No.21, pp. 5768-5772, ISSN 0022-2461

Wu, M. (2009). Study of effect of hydrogen on the properties of ferroelectric ceramics. Doctoral dissertation, University of Science and Technology Beijing.

Wu, M.; Huang, H. Y.; Chu, W. Y.; Guo, L. Q.; Qiao, L. J.; Xu, J. Y. & Zhang, T. Y. (2010). Tuning the ferroelectric and piezoelectric properties of 0.91Pb(Zn$_{1/3}$Nb$_{2/3}$)O$_3$-0.09PbTiO$_3$ single crystals and lead zirconate titanate ceramics by doping hydrogen. Journal of Physical Chemistry C, Vol.114, No.21, pp. 9955-9960, ISSN 1932-7447

Zhang, H.; Su, Y. J.; Qiao, L. J. & Chu, W. Y. (2008). The Effect of Hydrogen on the Fracture Properties of $0.8(Na_{1/2}Bi_{1/2})TiO_3$-$0.2(K_{1/2}Bi_{1/2})TiO_3$ Ferroelectric Ceramics. *Journal of Electronic Materials*, Vol.37, No. 3, pp.368-372, ISSN 0361-5235
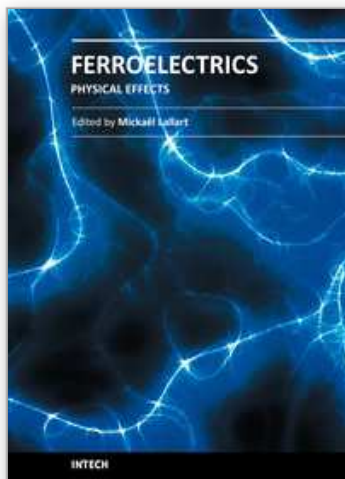
Ferroelectrics - Physical Effects

Edited by Dr. Mickaël Lallart

Ferroelectric materials have been and still are widely used in many applications, that have moved from sonar towards breakthrough technologies such as memories or optical devices. This book is a part of a four volume collection (covering material aspects, physical effects, characterization and modeling, and applications) and focuses on the underlying mechanisms of ferroelectric materials, including general ferroelectric effect, piezoelectricity, optical properties, and multiferroic and magnetoelectric devices. The aim of this book is to provide an up-to-date review of recent scientific findings and recent advances in the field of ferroelectric systems, allowing a deep understanding of the physical aspect of ferroelectricity.

How to reference

In order to correctly reference this scholarly work, feel free to copy and paste the following:

INTECH
open science | open minds